



TITLE:

# Flume experiments in the development of crevasse-splay deposits: transition from asymmetric-to-symmetric geometry

AUTHOR(S):

Kato, Taichi; Yamada, Masaki; Naruse, Hajime; Yuichi, Sakai

---

CITATION:

Kato, Taichi ...[et al]. Flume experiments in the development of crevasse-splay deposits: transition from asymmetric-to-symmetric geometry. *Journal of Sedimentary Research* 2023, 93(11): 825-839

ISSUE DATE:

2023-11

URL:

<http://hdl.handle.net/2433/286214>

RIGHT:

Accepted for publication in [Journal of Sedimentary Research] as of [11 Aug 2023]; This is not the published version. Please cite only the published version. この論文は出版社版ではありません。引用の際には出版社版をご確認ご利用ください。

**Flume experiments in the development of crevasse-splay deposits: Transition from asymmetric  
to symmetric geometry**

TAICHI KATO<sup>1</sup>, MASAKI YAMADA\*<sup>2</sup>, HAJIME NARUSE<sup>3</sup>, AND YUICHI SAKAI<sup>4</sup>

<sup>1</sup> *Geology Unit, Science Division, Department of Science, Graduate School of Science and  
Technology, Shinshu University, 3-1-1 Asahi, Matsumoto, Nagano 390-8621, Japan*

<sup>2</sup> *Department of Geology, Faculty of Science, Shinshu University, 3-1-1 Asahi, Matsumoto, Nagano  
390-8621, Japan*

<sup>3</sup> *Division of Earth and Planetary Sciences, Graduate School of Science, Kyoto University,  
Kitashirakawa-Oiwakecho, Sakyo-ku, Kyoto, Kyoto 606-8502, Japan*

<sup>4</sup> *Department of Forest Science, Utsunomiya University, 350 Mincho, Utsunomiya, Tochigi, 321-  
8505, Japan*

*e-mail: yamada@shinshu-u.ac.jp*

**ABSTRACT**

Crevasse-splay deposits play an important role in the reconstruction of the magnitude of past flood events and in understanding the behavior of river systems. Despite the extensive studies conducted on the geometry and facies of crevasse-splay deposits, their spatiotemporal developmental processes have remained insufficiently understood. In this study, scaled flume experiments were conducted to

study the relationship between the developmental processes of crevasse splays and their characteristics. An experimental flume was set up in a tank to simulate the 2019 Chikuma River flood, Central Japan event. To model the overbank flow, an opening was created on the side of the flume's wall through which the flow flooded onto a horizontal acrylic plate. The sediment used in the experiments consisted of particles with grain sizes of approximately 0.3 and 0.1 mm, which were determined to be equivalent to bedload gravel and suspended sand in a real-scale river using dimensional analysis. The results of the experiments revealed three important findings: (1) Crevasse-splay deposits initially developed an asymmetric shape extending downstream of the main river channel but gradually showed a symmetric geometry. The river mainstream initially influenced the direction of the inundation flow, but channel bifurcations after the deposition of the sediment piles later changed the geometry of splays into a more symmetric shape. (2) Crevasse-splay deposits developed in two distinct regions (proximal and distal splay), corresponding to sediment transport by bedload and suspended load, respectively. These two regions are commonly observed in the actual field scale. (3) The original overbank flow was a sheet flow without channels, which caused coarse-grained sediments to be spread over a wide area. Subsequently, the accumulation of coarse sands in the developed channel interiors resulted in the buildup of finer-grained sediments upstream of the proximal splay. Thus, the proximal splay deposits became slightly coarse downstream, whereas they rapidly became fine at the boundary with the distal splay. These findings indicate that the

characteristics of crevasse-splay deposits vary with the landform's development stage, thus providing a basis for interpreting their depositional facies.

## INTRODUCTION

Crevasse channels and splays play an important role in river systems, such as overbank deposition and channel avulsion (e.g., Smith et al. 1989; Aalto et al. 2002; Hajek and Edmonds 2014; Rahman et al. 2022). Earlier studies have described modern crevasse-splay deposits (e.g., Bristow et al. 1999; Florsheim and Mount 2002; Arnaud-Fassetta 2013; Matsumoto et al. 2016) and have also recognized different facies of crevasse-splay deposits in ancient deposits (e.g., Fielding 1984; Gugliotta et al. 2015; Gulliford et al. 2017; Chomiak 2020; Widera et al. 2023). For example, Rahman et al. (2022) examined and summarized the characteristics of a total of 1556 crevasse-splay deposits identified using satellite imagery from 1984 to 2020. Colombera and Mountney (2021) verified the influence of crevasse-splay deposits on sandbody connectivity using the combined data from ancient and modern crevasse-splay deposits. Toonen et al. (2016) described how a crevasse splay developed with an asymmetric morphology downstream of the main channel in the initial stage of its formation, and that the crevasse-channel orientation varied perpendicular to the main channel several decades later. Florsheim and Mount (2002) also observed a similar development of the crevasse splay from asymmetric to symmetric.



However, these studies were all based on observations of the geomorphological or sedimentary features that resulted from landform development and not direct observations of the spatiotemporal development of the landform itself. Toonen et al. (2016) described the asymmetric morphology of the crevasse-splay deposits in the initial stage of formation and the change of the crevasse-channel orientation using decades as the time scale. Therefore, their temporal development may occur progressively over a time period of several decades, making it challenging to clarify the process only from observations of modern or ancient deposits. Therefore, investigations employing numerical or physical experiments of crevasse splays are needed to reveal the governing factors on the development process of facies and topographic features.

Only a few studies have investigated in detail the flooding flow behavior on crevasse splays with depositional processes of mixed-grain-size sediment during a levee breach. Although many flume experiments associated with levee breaches have been conducted, most of them were performed without sediment supply, so the formative process and depositional features of crevasse-splay deposits were not recorded by those experiments (e.g., Yu et al. 2013; Satter et al. 2019; Özer et al. 2020). Some earlier studies conducted flume experiments of flooding flows that involved a sediment supply to understand the geomorphic features of the resultant deposits, but the formative processes of the crevasse-splay deposits were not described (e.g., Takahashi et al. 1984; Fujita et al. 1987; Takahashi and Nakagawa 1987; Tobita et al. 2015). Numerical modelings of the deposition involving

a levee breach have also been conducted (e.g., Takahashi and Nakagawa 1989; Yuill et al. 2016; Millard et al. 2017; Nienhuis et al. 2018; Li et al. 2023). For example, Millard et al. (2017) examined how channel-sediment size and flood-basin hydrology influence sediment transportation to the floodplain through crevasse splays. Li et al. (2023) reported that increases in discharge lead to more rapid splay sedimentation, and increases in floodplain water level result in shorter but wider splays. Yuill et al. (2016) demonstrated an erosional and depositional process during a levee breach using a coupled field observation and numerical modeling of crevasse-splay deposits at West Bay, Louisiana, USA. However, these studies did not examine the development process of the geomorphology and facies. Variation in grain-size distribution contributes to the interpretation of crevasse-splay facies in ancient deposits (Burns et al. 2017), which has not been explored in existing experimental or numerical studies of river flooding flows.

In this study, we aimed to understand the spatiotemporal development process of crevasse-splay facies. To this end, flume experiments were conducted to reproduce the distribution and sedimentary characteristics of crevasse-splay deposits formed when a levee is breached. The asymmetric-to-symmetric developments of the crevasse-splay geometry have already been reported in various studies (Florsheim and Mount 2002; Toonen et al. 2016). Here, our experiments verified whether this mode of development is a common feature for all crevasse splays. In the experiments, the focus was also on the relationship between the transition of facies and process change. Burns et al. (2017,

2019) suggested that crevasse-splay facies could be divided into proximal, medial, and distal splays. They implied that bedload-induced sedimentary structures characterize the proximal splays. By contrast, the distal splay deposits are mainly formed by suspension fallout. However, since these estimations have not yet been examined through direct observations, it is necessary to confirm this by the experiments.

For the experimental conditions, the nondimensionalized hydraulic and sedimentary conditions of the October 2019 flooding of the Chikuma River in Nagano Prefecture, central Japan (Yamada et al. 2023) was used. The gauging stations recorded the hydraulic conditions of the flooding event, whereas the field surveys revealed significant variations in the thickness and grain-size distributions of gravelly and sandy crevasse-splay deposits formed in the area of the breached levee (Yamada et al., 2023). Therefore, the conditions of this flooding event are suitable for constraining the flume experiments to better understand the processes involved in the transport and deposition of sediments during a flooding event. This study set the experimental conditions based on the dimensional analysis of the flooding so that the experimental crevasse splays were expected to have fluid properties similar to field-scale topography. However, the purpose of this study is not necessarily to reproduce the phenomena that occurred in a particular region. The experimental conditions mimicked a specific disaster because the flooding was a well-documented and common scale (Özer et al. 2020). In this paper, we interpret the experimental results as representing the universal features

of the developmental process of crevasse splays.

## GEOMORPHOLOGIC SETTING AND 2019 FLOOD EVENT

Crevasse-splay deposits were studied near the breached levee of the Chikuma River in the Hoyasu area, Nagano Prefecture, central Japan, by Yamada et al. (2023) (Fig. 1). The 30-m-wide levee revetment of the left bank of the river was breached for over a length of 70 m. As a result, crevasse-splay deposits were formed on both sides of the crevasse channel. The thickness of the upstream gravel-prone sediment pile was estimated to be a maximum of 2.5 m and 1.3 m on average. It consisted mainly of deposits ranging from cobbles to boulders, and covered an area of about 6630 m<sup>2</sup>. The thickness of the downstream sand-prone sediment pile was estimated to be a maximum of 1.1 m and 0.6 m on average, which included deposits ranging from pebbles to cobbles, and covering an area of about 4340 m<sup>2</sup>.

The Chikuma River in the study area has a width of about 920 m and a flow depth of about 5 m at the full bank discharge (Investigation Committee on the Chikuma River Levee, 2020). The average river slope in the study area is 0.1%, and the floodplain is approximately 2160 m wide. The time of overtopping and levee breach was calculated through a closed-circuit television camera placed on the levee and from the water-level records at the upstream and downstream gauging stations (Investigation Committee on the Chikuma River Levee 2020; Yamada et al. 2023). The river

water overflowed the levee revetment at 0:55 AM on October 13. The levee was then estimated to have been breached from 2:15 AM to 5:30 AM on October 13. The water level of the river gradually dropped over approximately 3 h after the initial levee breach happened.

## METHODS

### *Experimental Setting*

An experimental tank at Kyoto University was used to conduct flume experiments to model the crevasse channel and associated deposits at the study site. The experimental setup was designed to be an approximately 1/200 scale for the measured values of the river width and depth at the study site of Yamada et al. (2023). The flume was made of acrylic boards 8 cm wide and 20 cm high (Fig. 2). A 35-cm-wide sluice gate was placed on the right side of the middle part of the flume. This sluice gate modeled the broken part of the levee in the Chikuma River. The 35-cm-wide and a 20-cm-high acrylic plate or multiple 2-cm-high plates were placed inside the sluice gate. The floodplain was modeled using an acrylic board (150 cm wide and 100 cm long) and was placed outside the flume. It was painted in blue and then white-colored grid lines (10 cm grid in Runs 1–3 and 5 cm grid in Runs 4–6) were marked on it to measure and to collect samples at regular intervals. The slope of the floodplain board was changed from  $-1.4\%$  to  $0\%$  away from the flume.

A pipe was installed upstream of the flume as the inlet for a mixture of water and sand. Two

types of colored sand (green and red) were used in the experiments. The grain sizes of the green and red sands were 297 and 102  $\mu\text{m}$  in geometric mean diameter, respectively. Considering the similarity law, these sands are determined to reproduce the behavior of gravel and sand, respectively, at natural scales (described later). The board was installed perpendicular to the bottom at the downstream end to control the flow depth by narrowing the flow.

### ***Experimental Flow Conditions***

Water and the colored siliciclastic sand were mixed in the external tanks and injected at a constant flow discharge through the inlet to the flume. After the flow in the flume achieved a steady state, the acrylic plates at the sluice gate were removed to simulate the levee breach. The reproduction of the levee breach process was changed by the type of acrylic boards installed in the sluice gate. A single large board (35 cm wide and 20 cm high) was used to reproduce an immediate breach (Fig. 3A), whereas 2-cm-high boards (hereinafter referred to as small board) were used to reproduce a gradual breach (Fig. 3B, C). The experiment times (start of overflow and levee breach) were also changed in addition to the breach patterns.

Six experiments (Runs 1–6) were conducted, and the hydrograph of the overflowing current was changed by removing the acrylic plates of the sluice gate. Levee breach occurred following three patterns: (A) removing the large board to cause an instantaneous breaching of the levee (Fig. 3A),

(B) removing three small boards sequentially to cause gradual breaching (Fig. 3B), and (C) removing the first small board, and then removing second and third boards at the same time to simulate the breaching process in the Chikuma River (Fig. 3C). In patterns B and C, the first board was removed to reproduce the overflowing stage of the flooding, and the remaining small boards were removed to reproduce the levee breach (Fig. 3B, C). The last small board remained in the bottom of the sluice gate. Other conditions, such as time of the experiment and the slope of the floodplain, were changed in each experiment (Table 1).

A mixture of water and sediment (red and green sands) were sampled from the external mixing tank and the downstream end of the flume to determine the sediment concentration in the flow. The concentration in the mixing tank and downstream edge were measured (Table 1). The quantity of flow per unit time was  $925.7 \text{ cm}^3/\text{s}$  ( $9.26 \times 10^{-4} \text{ m}^3/\text{s}$ ).

### *Measurements and Sampling*

The surface velocity of flood flow at the time of overflow, immediately after the levee breach, and 60 s after the levee breach was measured by letting styrene foams float on the flood flow during the experiments (see Supplement 1). After each of the experiments in Runs 2–6, approximately 20 photographs were taken by a camera (Nikon D7000) to cover and overlap the entire formed deposit for image analysis measuring the sediment thickness. The image analysis was conducted by the

software, Agisoft Metashape Professional, using the Structure from Motion-Multi View Stereo method (Remondino et al. 2014). The digital elevation models (DEMs) and orthophotos were produced with georeferencing points at the grids of the white lines on the acrylic board. In addition, the formation process of deposits during all runs was observed using video images taken by two fixed-point cameras (Nikon D7000) (Supplement 1). One was placed approximately 1 m above the floodplain board to take a video from above. The other one was placed approximately 3.5 m from the flume to capture panoramic video.

After experimental Runs 4 and 6, sediment samples were collected at every 5-cm grid. The collected samples were sieved to separate the fine (red) and the coarse (green) sands, and the dry weights of these sands were measured. The volume per unit area of the sediment was calculated from the dry weight in the total and density (using  $2.7 \text{ g/cm}^3$  of common quartz). The ratio of green sand in the total was also calculated to understand the trends of grain-size distribution.

### ***Scaling for the 2019 Chikuma River Flooding***

This study compares the experimental conditions to the hydraulic conditions in the 2019 Chikuma River flooding through the Froude number and Shields dimensionless stress.

The Froude number is defined as



$$Fr = \frac{U}{\sqrt{gh}} \quad (1)$$

where  $U$  and  $h$  denote the depth-averaged velocity and the flow depth, respectively, and  $g$  is the acceleration of gravity. Under turbulent conditions, where the Reynolds number  $Re = Uh/\nu$  ( $\nu$  denotes the kinematic viscosity of water) is sufficiently large ( $Re \gg 2000$ ), if the Froude number is equivalent, the fluid in the experimental conditions is expected to exhibit behavior similar to the actual flood.

To determine the behavior of the transported sediment, the Shields dimensionless stress is used to examine the similarity between the experimental and natural phenomena. This parameter takes the form

$$\tau_* = \frac{u_*^2}{RgD} \quad (2)$$

where  $R = (\rho_s - \rho)/\rho$  ( $\rho_s$  and  $\rho$  are the density of the sediment and water, respectively) is the submerged specific density of the sediment.  $D$  denotes the representative grain size of the sediment,

and  $u_*$  indicates the friction velocity, estimated by the following equation:

$$u_*^2 = C_f U^2 \quad (3)$$

where  $C_f$  is the bed friction coefficient, which can be estimated using the following relation:

$$C_f = \left( \frac{1}{\kappa} \log 11 \frac{h}{k_s} \right)^{-2} \quad (4)$$

The parameter  $\kappa$  (0.4) and  $k_s$  denote the von Kármán constant and the bed roughness height,

respectively. In this study, the bed roughness height,  $k_s$ , is obtained by

$$k_s = \alpha D \quad (5)$$

where  $\alpha$  is an empirical parameter that is set to 6.6 following Hammond et al. (1984).

Another dimensionless number of interest with respect to the mode of sediment transport is the

suspension index,  $I_s$ , which is defined as

$$I_s = \frac{u_*}{W_s} \quad (6)$$

where  $W_s$  is the settling velocity of the sediment particle (Ferguson and Church 2004). It is known

that suspended sand transport is dominant when  $I_s$  is approximately greater than 1 (Niño et al.

2003).

## RESULTS

### *Similarity in the Hydraulic Parameters*

This study conducted six experiments in total (Runs 1–6; Fig. 4). In all experiments, the model

Froude number  $Fr_m$  and the model Shields number  $\tau_{*m}$  in the flume were comparable to those in

the Chikuma River during the actual flooding event (Table 2).

In all runs, the Froude number in the flume,  $Fr_m$ , was 0.29 during the experiment, whereas the

Froude number in the Chikuma River,  $Fr_p$ , during the actual flood was 0.29 (Table 2), which is

equal to the experimental value. As for the values of Shields dimensionless stress, the value in the

flume,  $\tau_{*m}$ , was 0.0505 and 0.147, when the representative grain size during the experiment was 297

$\mu\text{m}$  (green sand) and 102  $\mu\text{m}$  (red sand), respectively. Although it is not easy to accurately estimate

the representative grain size during flooding in the Chikuma River, Yamada et al. (2023) reported

that the approximate median gravel size consistent with a crevasse splay was about 5.0 cm. Using

this diameter, the value of Shields dimensionless stress,  $\tau_{*p}$ , in Chikuma River is estimated to be

0.0566, which is close to that for the green sand in the experimental flume.

The suspension index,  $I_s$ , for the green and red sands were 0.321 and 1.89, respectively. Thus,

the latter exceeded the suspension threshold, indicating that the fine-grained red sand was transported as a suspended load in the flume.

### ***Behavior of Flooding Flows***

The behavior of flooding flows on the experimental overbank varied through three stages: overflowing, breaching, and branching. In all experimental runs, except for Runs 1 and 2, the overflow current from the flume initially happened by removing the first plate in the sluice gate (the overflowing stage). In this stage, the overflowing current was almost perpendicular to the main flume flows. After this stage, the levee breach was simulated by removing the remaining plates, and the direction of the flood flow shifted downstream as the levee breach progressed (the breaching stage). After the crevasse splay developed from the flood flow, the crevasse channels branched (the branching stage), and the radial-shaped crevasse splays were formed from the flows except for Runs 1 and 2.

The deposition of fine-grained sediment characterizes the initial stage of the overflowing current. Figure 5 shows the behavior of the flood flows in Run 4. The first plate in the sluice gate was removed to commence the overflowing current at 59 s after the experiment started. At this early

stage of flooding, the overflowing current was oriented toward  $65^\circ$  downstream with a velocity of 35 cm/s (Figs. 5A, 6). Here, the flow direction is expressed by the clockwise angle from downstream of the main flume (Fig. 5). The fine-grained particles (red sand) were deposited on both sides of the overflowing current in this stage, establishing the crevasse channel on the overbank region (Fig. 5A).

Then, the levee breach caused an intense flood flow on the overbank. The second and third plates were removed simultaneously at 87 s after Run 4 started, and thus the discharge of the flood flow suddenly increased (Pattern C). The flow velocity in the crevasse channel increased to 81 cm/s as a result (Fig. 6). The coarser-grained sediment (mixture of green and red sands) was then deposited in broad regions on the upstream side of the crevasse channel (Fig. 5B).

The direction of the crevasse channel migrated downstream as a result of the development of the sediment pile in the upstream region. The crevasse channel oriented  $56^\circ$  from the downstream direction at around 117 s after the experiment commenced (Fig. 5C). The flow velocity was then slightly reduced (67 cm/s at 177 s after the experiment started; Fig. 6), and the upstream pile continued to grow toward the downstream side (Fig. 5D). Because of the development of the upstream sediment pile, the channel direction further migrated toward the downstream side. The crevasse channel was oriented at  $40^\circ$  from the downstream direction at 207 s after the experiment started (Fig. 5D). The sediment pile on the downstream side of the crevasse channel also developed gradually after the upstream pile grew. However, as the channel gradually shifted downstream, the

downstream sediment pile was partially eroded, and the overall development of the pile was lesser than that in the upstream region (Fig. 5D).

Along with the main crevasse channel described earlier, a minor branched channel also developed in the upstream direction ( $103^\circ$ ), and a small pile was formed from this minor channel (Fig. 5C, D). From around 143 s after the experiment commenced, the third branch crevasse channel began to form between the piles of the minor and main channels, resulting in the development of thin piles. These piles constituted the resultant radial shape of the crevasse splay (Fig. 5D). At this stage, the finer-grained sediment, which was composed mainly of red sand, was deposited above the coarser-grained sediment formed in the breaching stage.

The behavior of the overflowing current resembled Run 4 in all runs, whereas the mode of the downstream pile development varied depending on the pattern of the experimental conditions (Figs. 7–9). The downstream pile was eroded once in Runs 1 and 2. The overflowing current and the levee breach progressed instantaneously in these runs (Pattern A). The flume-channel floor in the downstream region from the sluice gate was entirely exposed due to the degradation of the bottom sediment. Unlike other runs, the channel branching on the crevasse splay did not occur in Runs 1 and 2 (Fig. 7A). The flooding flow of Runs 1 and 2 decelerated within a shorter time than the other runs, and the downstream sediment pile was redeveloped in the final stage of the decay of the flooding flow in these runs. The patterns of the levee breach in Runs 3, 5, and 6 were mostly the same as in

Run 4. However, in Runs 3 and 5, the experiment duration after the levee breach was about 1 min shorter than in Runs 4 and 6 (Table 1). The development of the downstream pile was much weaker than in other runs.

### *Depositional Features of the Crevasse-Splay Deposit*

Two major regions were discovered in the crevasse splay: the proximal and the distal splays. The proximal splays were composed of coarse-grained green and fine-grained red sands (Figs. 7–9). They were relatively thick (about 10–15 mm maximum), and consisted of more than one sediment piles (Figs. 7–9). The distal splays were very thin ( $< 1$  mm) and exhibited a sheet-like geometry (Figs. 7–9). The boundary between the proximal- and distal-splay regions was clearly defined, where the deposit thickness abruptly changed (Fig. 10).

Each sediment pile in the proximal splays exhibited lobate geometry that elongated downstream in all runs. The long axis of the sediment piles ranged from  $25^\circ$  to  $46^\circ$  from the downstream direction. The peaks of piles located in the region from the upstream end to the center of the sediment piles gradually thinned downstream. Image analysis of the topography indicated that the maximum thickness of the crevasse splay was below 15 mm.

In the proximal splays, two prominent sediment piles along both sides of the crevasse channel were revealed after the experimental runs. The upstream pile tended to be thicker than the

downstream pile in all the runs (Figs. 7–10). Also, several minor piles developed in Runs 3–6. The maximum volumes per unit area of the upstream and downstream piles ranged from 5.9 to 6.7 mm and 4.5 to 5.7 mm, respectively. The total area of both piles ranged from about 2650 to 2670 cm<sup>2</sup> and about 874 to 1150 cm<sup>2</sup> (Figs. 7–9), respectively. The volume per unit area along transect P–P' parallel to the main channel decreased away from the center of the pile. It also decreased distinctly as a function of distance from the main channel (Fig. 10).

Smaller piles also developed in the upstream direction around the branched minor crevasse channels. A single small pile was observed in Run 3, and two small piles extended perpendicular to the main flume flows were recognizable in Runs 4–6. The area of these small piles ranged from about 481 to 794 cm<sup>2</sup> (Figs. 7B, C, 8, 9).

The weight ratios of the coarse-grained green sand to fine-grained red sand were examined to determine the grain-size distribution in the experimental deposits of Runs 4 and 6 (Figs. 8D, 9D). The ratio of the coarse-grained green sand to the fine-grained red sand generally increases from the center toward the edges of the piles in the crevasse splay, indicating a coarsening trend toward the crevasse channels and the terminal ends of the piles. As described earlier, the deposit thickness becomes abruptly thin, and a lower green-sand ratio was observed on the left and right edges of the splays on the floodplain.

A video recording indicated that the migration of the depocenter on the floodplain caused a



coarsening trend downstream in the proximal crevasse splay described earlier. In the levee-breaching stage, the unconfined intense flooding flows distributed the coarse-grained sediment on the broad regions of the floodplain, forming the basal part of the proximal splay. Then, in the branching stage, the relatively finer-grained sediment was accumulated in the upstream regions of the sediment piles by the flow overflowing from the established crevasse channel. As a result, the proximal splay deposit exhibited a fining-upward trend in the vertical sections. In plan views, the deposits became coarse downstream toward the fringes of the splay where the basal part of the splay deposits was exposed.

Comparing the grain sizes of the upstream and downstream sediment piles, the spatially averaged ratios of the coarse green sand were 38.4% and 38.2% for the upstream and downstream piles in Run 4, respectively. In the case of Run 6, these values were 47.2% and 43.0%, respectively. Thus, the upstream pile was coarser than the downstream pile in Run 6, while they were identical in grain size in Run 4. In this comparison, the data obtained from the grid point where the bed thickness was less than 1 mm was ignored.

## DISCUSSIONS

### *Formative Process of Crevasse Splay*

As a result of Runs 3–6 in this study, the sediment piles in the crevasse splays were initially

oriented perpendicular to the main channel in the overflowing stage, and subsequently, the crevasse channel and the sediment pile shifted to the downstream side in the levee breaching stage (Fig. 5). Finally, the crevasse channel branched to form the radial shape of the crevasse splay. Although it was not explicitly described, the deposition of the sediment pile on the upstream side of the overbank and the change in the flood flow direction were also observed in the levee-breaching experiment of Yamasaka and Kubota (2002). The initial sediment pile in the overflowing stage was formed due to the lateral expansion of the flows that reduces the flow velocity. Later, the direction of the crevasse channel shifted because the sediment pile developed enough to block the flood flow. This migration of the crevasse channel direction initially becomes oriented downstream in response to the flow direction of the main channel. Subsequently, the sediment pile is breached where the flood flow is bent so that the bifurcation of the crevasse channel occurs in the final branching stage.

The formative processes in this study exhibit similarity to those of the mouth bars in delta systems in other studies (e.g., Edmonds and Slingerland 2007; Ahmed et al. 2014). Feng et al. (2019) described that river mouth bars were formed at the ends of the channels. In the latter stage of their experiment, the channel branched because the river flow was blocked by the mound of the mouth bar formed in the early stage. Similar processes can also be observed in modern deltaic systems (e.g., Wright 1973; Fan et al. 2006). The formative process observed in this study is similar to the example of the mouth bar (Toonen et al. 2016). The crevasse channel shifted downstream because of the

blockage by the pile formed on the upstream side. Yamasaka and Kubota (2002) also described the deposition on the upstream side and the change in the flooding flow direction in the flume experiment.

However, the crevasse-splay features differ from the mouth bars with respect to the symmetry between the upstream and downstream sides. In the case of crevasse splays, the branched crevasse channels develop earlier on the downstream side and are more prominent than the channels oriented upstream. In contrast, the branched channels in the river mouth bars in delta systems are nearly symmetric. This difference is because the flows in the main channels affect the direction of the flood flows. Rahman et al. (2022) reported similar asymmetric features of crevasse splays. They described that the crevasse-splay orientation to the flow direction in the parent channel was  $75^\circ$  on average in a total of 1556 measurements. The direction of crevasse splays ranged from  $10^\circ$  to  $140^\circ$ , and 64% of the data were less than  $90^\circ$ . The direction of crevasse-splay deposits observed in the experiments in this study were oriented mainly downstream, the features of those deposits correspond to that of general crevasse-splay deposits.

The development processes of experimental deposits in this study were also observed in modern crevasse-splay deposits. Toonen et al. (2016) indicated that the modern crevasse channel in the Cumberland Marshes in Canada was initially bent downstream under the influence of the main river flow, while becoming oriented downstream after the slope of the splay fully developed. They

reported that the crevasse splay develops through three stages: the initial levee breach, the crevasse-splay formation, and the splay termination. In the crevasse-splay formation stage, the crevasse channel initially oriented downstream of the main channel. This asymmetric development of the splay was due to the obstruction of the developed sand sheets. Later, the angle between the main river channel and the elongation direction of the splay increased to 90° at maximum because of the blockage caused by the previously deposited splay sand sheets. These transitions of the crevasse-channel orientation are similar to those observed in the experimental results of this study. Thus, in the experiments, we concluded that the asymmetric-to-symmetric development is typical of crevasse channels and splay developments.

### *Characteristic Features of the Crevasse-Splay Deposit*

The experimental deposits in this study can be divided into two regions: the thick coarse-grained proximal splay and the thin fine-grained distal splay (Figs. 7–9). The abrupt change in thickness and grain size of deposits occurred between these two regions. Similar topographic changes in the crevasse splays have been recognized in other field observation studies (e.g., Burns et al. 2017; Gulliford et al. 2017). Burns et al. (2017) investigated ancient crevasse-splay deposits at 35 locations in the Cretaceous Castlegate Sandstone and Nelson Formation of the Mesaverde Group, eastern Utah, USA, and characterized proximal splays as a wedge-shaped geometry with thick and coarse-

grained deposits. They exhibit a sedimentary structure induced by the bedload sediment transport. In contrast, the distal splay is characterized by a planar-shaped geometry with thin fine-grained deposits. Burns et al. (2017) reported that distal splay deposits rarely contain sedimentary structures, such as ripples or dune cross-lamination. It was inferred that the bedload transport process is dominant in the proximal splay, whereas deposits in the distal splay are predominantly formed by suspension fallout (Burns et al. 2017).

We infer that the transition of the sediment transport process from the proximal to the distal splay also occurred in our experiments. The video recording of the experiments as well as the suspension indices calculated from the flume hydraulic conditions showed that the bedload layer carried the coarser green sand, while the finer red sand was carried mainly as the suspended load. Therefore, it is implied that the transition between the two splay regions occurred where the shear stress of the flooding flow reached below the threshold of the bedload sediment motion (Ikeda 1982). The change in the sedimentary facies observed in the field also occurred in this study, although the bedload sedimentary structure was not observed in our experiments due to the scaling issue.

Inside the proximal splay deposits, a coarsening trend toward the crevasse channels and the terminal end of the piles was observed in this study, resulting from the gradual development of the channel architectural element. The same trend was also observed in other studies on modern and experimental deposits (e.g., Takahashi et al. 1984; Bristow et al. 1999; Tobita et al. 2015). The

experimental observations imply that this trend is caused by the initial dispersal of the coarse-grained sediment because the confinement of the crevasse channel was not fully developed at this stage. Later, the flood flows were confined to the developed channels, so the finer sediment accumulated above the coarse-grained deposits in the upstream region of the proximal splay. As a result, they did not always become finer downstream inside the proximal splay region because of the transition from the unconfined flooding to the confined channel flows. Thus, the change in the depositional processes in succession needs to be carefully studied to interpret the proximity of facies from the grain-size trends in ancient crevasse-splay deposits.

Finally, it should be noted that the asymmetric development of the crevasse splay described previously affects the depositional features of the splay deposits. The deposits of the upstream pile were thicker than those of the downstream pile because they were eroded by the crevasse channel shifting toward the downstream side. In addition, the upstream pile was coarse grained because initial unconfined flooding formed the central part of this pile, while the downstream pile was formed from the overflowing current from the confined crevasse-channel flows. The same feature was observed in the Hoyasu area (Yamada et al. 2023). Other studies also described the same feature (e.g., Florsheim and Mount 2002; Arnaud-Fassetta 2013). Thus, the experimental and field observations revealed that crevasse splays develop from asymmetric-to-symmetric plan shapes in their geometry, suggesting that the three-dimensional reconstruction of the facies of ancient

crevasse-splay deposits could imply the development stage of the splays.

Although the experiments in this study considered the general features of the development process of crevasse splays on flat basin plains, the actual splays are affected by geomorphological conditions, such as the slope of basins or local obstacles, including artificial structures. Several studies have suggested that the basin slope influences the mode of the splays. For example, Gębica and Sokołowski (2001) determined that the shapes of crevasse splays vary due to surface morphology. In addition, local obstacles may fundamentally change the development process of crevasse channels. For example, the crevasse channel observed in the 2019 flooding of the Chikuma River was oriented perpendicular to the main channel, whereas the channels generally are oriented downstream in the basins, as observed in the flume experiment of this study (Takahashi et al. 1984; Yamasaka and Kubota 2002; Tobita et al. 2015; Matsumoto et al. 2016; Rahman et al. 2022; Fig. 5). In the case of the Chikuma River, the direction of the crevasse channel was forced by an artificial structure near the breached location. Other studies have also implied that local topography and obstacles are not negligible factors in the entire development modes of the crevasse splays (e.g., Gębica and Sokołowski 2001; Toonen et al. 2016). Thus, additional experiments with various topographic conditions, including gradients of the main river channel and floodplains, are expected to reveal the diversity and general understanding of the formative process of crevasse-splay deposits.

### *Implications for Analyses of Geologic Records*

Here, we discuss the contribution of our experimental results to the analysis of ancient deposits.

To identify crevasse-splay facies from strata with a high degree of certainty, their architectural elements and developmental stages must be inferred from sedimentary structures (e.g., Hornung and Aigner 1999; Burns et al. 2017).

The distribution of paleocurrent direction can be the key to identifying the developmental stages of crevasse splays in ancient deposits (Burns et al. 2017). Judging from the experimental results, the directions of flows that deposited them have a uniform directional distribution preferentially oriented downstream if the crevasse splays are in the early stages of development. On the other hand, the distribution of paleocurrent directions of the flooding flows over the crevasse splay, which has acquired a radial shape in the later stages, is expected to be diverse and to show a wide range of directional distribution.

Identifying the developmental stage of the crevasse splay is related to estimating the stability of fluvial landforms (Li and Bristow 2015; Nienhuis et al. 2018). In the case of rivers with insufficiently developed natural levees, overflows occur at many locations, so crevasse splays should be repeatedly abandoned in the early stages of their development. In contrast, in rivers with muddy and stable natural levees that occasionally flood heavily, crevasse splays should be maintained for an extended period, and the late-stage splays with radially distributed crevasse channels should



develop because the levee failures occur repeatedly in the same location.

In addition to the above, the experimental results of this study also have implications for estimating the spatial scale of crevasse splays. The experimental results confirm that the two previously proposed architectural elements of crevasse splay, proximal and distal splay (Burns et al. 2017), can be associated with transitioning processes from bedload to suspended-load sedimentation. This observation implies that the spatial scale of the distal splay, where only sedimentation from the suspended load dominates, is determined by the advection length. The distance that the flow travels before all the suspended load has settled is called the advection length, defined as the flow discharge divided by the settling velocity (e.g., Ganti et al. 2014). Thus, the spread of the distal splay can be predicted if the inundation flow can be estimated. Estimating the scale of sandy deposits such as crevasse sprays is not only for evaluating the past scale of flood events but also essential for exploration of hydrocarbon reservoir rocks (Anderson, 2005).

## CONCLUSIONS

In this study, scaled flume experiments were conducted to investigate the relationship between the developmental processes of crevasse splays and their characteristics. The results of the experiments can be summarized in the following three key findings:

(1) The crevasse-splay deposits in this study transformed from an asymmetric shape extending

downstream of the main river channel into a radial, symmetric geometry through the branching of the crevasse channels. During the initial overflowing stage, the fine-grained sand was uniformly spread on the floodplain, but this symmetry was disrupted in the breaching stage of the levee when the mainstream flow of the river altered the direction of the inundation flow, causing the crevasse splay to become asymmetric. As sediment piles accumulated and channel bifurcations occurred, the splay's geometry gradually evolved into a more symmetric shape.

(2) The experimental crevasse-splay deposits can be divided into two distinct regions (proximal and distal splays), which correspond to sediment transport by bedload and suspended load, respectively.

The proximal splay consisted of several crevasse channels and intervening sediment piles. In contrast, the distal splay was relatively smooth and consisted of thin suspended-load deposits.

(3) The proximal splay deposits exhibited a slight coarsening downstream, while they became rapidly fine at the boundary with the distal splay. During the original overbank flow, the absence of channels resulted in a sheet flow that distributed coarse-grained sediments over a broad region; however, as channels formed and accumulated the coarse sand in their interiors, slightly finer-grained sediment accumulated upstream of the proximal splay.

The findings in this study indicate that the characteristics of crevasse-splay deposits vary with time and space. The geomorphological development stage should be fully considered when interpreting the crevasse splay's sedimentary facies and paleocurrent directions.

## SUPPLEMENTAL MATERIAL

Supplemental files (experiment videos) are available from the SEPM Data Archive:

## ACKNOWLEDGMENTS

This work was partly supported by the Institute for Mountain Science, Shinshu University (T. Tokiwa) and JSPS KAKENHI Grant Number 20H01985 (H. Naruse). We thank Z. Cai and T. Nagato (Kyoto University) for supporting the experiments. Most of the figures were generated by Generic Mapping Tools (Wessel et al. 2019). The authors would like to thank Enago ([www.enago.jp](http://www.enago.jp)) for the English-language review. This paper was improved by reviews from Nigel Mountney, an anonymous reviewer, and Corresponding Editor John B. Southard.

## REFERENCES

- Aalto, R., Dunne, T., Nittrouer, C.A., Maurice-Bourgoin, L., and Montgomery, D.R., 2002, Fluvial transport of sediment across a pristine tropical foreland basin: channel–flood plain interaction and episodic flood plain deposition: The Structure, Function and Management Implication of Fluvial Sedimentary Systems, v. 276, p. 339–344.
- Ahmed, S., Bhattacharya, J.P., Garza, D.E., and Li, Y., 2014, Facies architecture and stratigraphic evolution of a river-dominated delta front, Turonian Ferron Sandstone, Utah, USA: *Journal of*

Sedimentary Research, v. 84, p. 97–121, doi:10.2110/jsr.2014.6.

Anderson, D.S., 2005, Architecture of crevasse splay and point-bar bodies of the nonmarine Iles Formation north of Rangely, Colorado: Implications for reservoir description: The Mountain Geologist, v. 42, p. 109–122.

Arnaud-Fassetta, G., 2013, Dyke breaching and crevasse-splay sedimentary sequences of the Rhone Delta, France, caused by extreme river-flood of December 2003: Supplementi di Geografia Fisica e Dinamica Quaternaria, v. 7–26, p. 8–26, doi:10.4461/GFDQ.2013.36.1.

Bristow, C.S., Skelly, R.L., and Ethridge, F.G., 1999, Crevasse splays from the rapidly aggrading, sand-bed, braided Niobrara Rivere, Nebraska: effect of base-level rise: Sedimentology, v. 46, p. 1029–1047, doi:10.1046/j.1365-3091.1999.00263.x.

Burns, C.E., Mountney, N.P., Hodgson, D.M., and Colombera, L., 2017, Anatomy and dimensions of fluvial crevasse-splay deposits: Examples from the Cretaceous Castlegate Sandstone and Neslen Formation, Utah, U.S.A: Sedimentary Geology, v. 351, p. 21–35, doi:10.1016/j.sedgeo.2017.02.003.

Burns, C.E., Mountney, N.P., Hodgson, D.M., and Colombera, L., 2019, Stratigraphic architecture and hierarchy of fluvial overbank splay deposits: Geological Society of London Journal, v. 176, p. 629–649, doi:10.1144/jgs2019-001.

Chomiak, L., 2020, Crevasse splays within a lignite seam at the Tomiślawice opencast mine near Konin, central Poland: architecture, sedimentology and depositional model: Geologos, v. 26,

p. 25–37, doi:10.2478/logos-2020-0002.

Colombera, L., and Mountney, N.P., 2021, influence of fluvial crevasse-splay deposits on sandbody connectivity: Lessons from geological analogues and stochastic modelling: *Marine and Petroleum Geology*, v. 128, p. 1–23, doi:10.1016/j.marpetgeo.2021.105060.

Edmonds, D.A., and Slingerland, R.L., 2007, Mechanics of river mouth bar formation: Implications for the morphodynamics of delta distributary networks: *Journal of Geophysical Research*, v. 112, no. F02034, doi:10.1029/2006JF000574.

Fan, H., Huang, H., Zeng, T.Q., and Wang, K., 2006, River mouth bar formation, riverbed aggradation and channel migration in the modern Huanghe (Yellow) River delta, China: *Geomorphology*, v. 74, p. 124–136, doi:10.1016/j.geomorph.2005.08.015.

Feng, W.J., Zhang, C.M., Yin, T.J., Yin, Y.S., Liu, J.L., Zhu, R., Xu, Q.H., and Chen, Z., 2019, Sedimentary characteristics and interal architecture of a river-dominated delta controlled by autogenic process: implications from a flume tank experiment: *Petroleum Science*, v. 16, p. 1237–1254, doi:10.1007/s12182-019-00389-x.

Ferguson, R.I., and Church, M., 2004, A simple universal equation for grain setting velocity: *Journal of Sedimentary Research*, v. 74, p. 933–937, doi:10.1306/051204740933.

Fielding, C.R., 1984, Upper delta plain lacustrine and fluvio-lacustrine facies from the Westphalian of the Durham coalfield, NE England: *Sedimentology*, v. 31, p. 547–567, doi: 10.1111/j.1365-3091.1984.tb01819.x.

- Florsheim, J.L., and Mount, J.F., 2002, Restoration of floodplain topography by sand-splay complex formation in response to intentional levee breaches, lower Cosumnes River, California: *Geomorphology*, v. 44, p. 67–94, doi:10.1016/S0169-555X(01)00146-5.
- Fujita, Y., Muramoto, Y., and Tamura, T., 1987, On the inflow of river water and sediment due to levee breach: *Disaster Prevention Research Institute Annuals at Kyoto University*, v. 30, p. 527–549 (in Japanese with English abstract).
- Gębica, P., and Sokołowski, T., 2001, Sedimentological interpretation of crevasse splays formed during the extreme 1997 flood in the upper Vistula River Valley (south Poland): *Annales Societatis Geologorum Poloniae*, v. 71, p. 53–62.
- Gugliotta, M., Flint, S.S., Hodgson, D.M., and Veiga, G.D., 2015, Stratigraphic record of river-dominated crevasse subdeltas with tidal influence (Lajas Formation, Argentina): *Journal of Sedimentary Research*, v. 85, p. 265–284, doi:10.2110/jsr.2015.19.
- Gulliford, A.R., Flint, S.S., and Hodgson, D.M., 2017, Crevasse splay processes and deposits in an ancient distributive fluvial system: The lower Beaufort Group, South Africa: *Sedimentary Geology*, v. 358, p. 1–18, doi:10.1016/j.sedgeo.2017.06.005.
- Hajek, E.A., and Edmonds, D.A., 2014, Is river avulsion style controlled by floodplain morphodynamics?: *Geology*, v. 42, p. 199–202, doi:10.1130/G35045.1.
- Hammond, F.D.C., Heathershaw, A.D., and Langhorne, D.N., 1984, A comparison between Shields' threshold criterion and the movement of loosely packed gravel in a tidal channel:

Sedimentology, v. 31, p. 51–62, doi:10.1111/j.1365-3091.1984.tb00722.x.

Hornung, J., and Aigner, T., 1999, Reservoir and aquifer characterization of fluvial architectural elements: Stubensandstein, Upper Triassic, southwest Germany: *Sedimentary Geology*, v. 129, p. 215–280, doi: 10.1016/S0037-0738(99)00103-7.

Ikeda, S., 1982, Incipient motion of sand particles on side slopes: American Society of Civil Engineers, *Journal of the Hydraulics Division*, v. 108, p. 95–114, doi:10.1061/JYCEAJ.0005812.

Investigation Committee on the Chikuma River Levee, 2020, A report of the Investigation Committee on the Chikuma River Levee (in Japanese and original title translated): 80 p, <https://www.hrr.mlit.go.jp/river/chikumagawateibouchousa/index.html> (in Japanese).

Li, J., and Bristow, C.S., 2015, Crevasse splay morphodynamics in a dryland river terminus: Río Colorado in Salar de Uyuni Bolivia: *Quaternary International*, v. 377, p. 71–82, doi: 10.1016/j.quaint.2014.11.066.

Li, J., Vegt, H., Storms, J.E.A., and Tooth, S., 2023, Crevasse splay morphodynamics near a non-vegetated, ephemeral river terminus: Insights from process-based modelling: *Journal of Hydrology*, v. 617, no. 129088, doi:10.1016/j.jhydrol.2023.129088.

Matsumoto, D., Sawai, Y., Yamada, M., Namegaya, Y., Shinozaki, T., Takeda, D., Fujino, S., Tanigawa, K., Nakamura, A., and Pilarczyk, J., 2016, Erosion and sedimentation during the September 2015 flooding of the Kinu River, central Japan: *Scientific Reports*, v. 6, no. 34168,

doi:10.1038/srep34168.

Millard, C., Hajek, E., and Edmonds, D.A., 2017, Evaluating controls on crevasse-splay size:

Implications for floodplain-basin filling: *Journal of Sedimentary Research*, v. 87, p. 722–739,

doi: 10.2110/jsr.2017.40.

Nienhuis, J.H., Törnqvist, T.E., and Esposito, C.R., 2018, Crevasse splays versus avulsions: A recipe

for land building with levee breaches: *Geophysical Research Letters*, v. 45, p. 4058–4067,

doi: 10.1029/2018GL077933

Niño, Y., Lopez, F., and Garcia, M., 2003, Threshold for particle entrainment into suspension:

*Sedimentology*, v. 50, p. 247–263, doi:10.1046/j.1365-3091.2003.00551.x.

Özer, I.E., Damme, M., and Jonkman, S.N., 2020, Towards an International Levee Performance

Database (ILPD) and Its Use for Macro-Scale Analysis of Levee Breaches and Failures:

*Water*, v. 12, no. 119, doi:10.3390/w12010119.

Rahman, M.M., Howell, J.A., and Macdonald, D.L.M., 2022, Quantitative analysis of crevasse-splay

systems from modern fluvial setting: *Journal of Sedimentary Research*, v. 92, p. 751–774,

doi:10.2110/jsr.2020.067.

Remondino, F., Spera, M.G., Nocerino, E., Menna, F., and Nex, F., 2014, State of the art in high

density image matching: *The Photogrammetric Record*, v. 29, p. 144–166, doi:

10.1111/phor.12063.

Satter, A.M.A., Bonakdari, H., Gharabaghi, B., and Radecki-Pawlik, A., 2019, Hydraulic Modeling



- and Evaluation Equations for the Incipient Motion of Sandbags for Levee Breach Closure  
Operations: *Water*, v. 11, no. 279, doi:10.3390/w11020279.
- Smith, N.D., Cross, T.A., Dufficy, J.R., and Clough, S.R., 1989, Anatomy of an avulsion:  
*Sedimentology*, v. 36, p. 1–23, doi:10.1111/j.1365-3091.1989.tb00817.x.
- Takahashi, T., and Nakagawa, H., 1987, Suspended sediment deposition in flood zones due to river  
bank breach: *Disaster Prevention Research Institute Annuals at Kyoto University*, v. 30, p.  
597–609 (in Japanese with English abstract).
- Takahashi, T., and Nakagawa, H., 1989, Simulation method on sedimentation in a protected low-land  
due to river bank breach: *Disaster Prevention Research Institute Annuals at Kyoto University*,  
v. 32, p. 733–756 (in Japanese with English abstract).
- Takahashi, T., Nakagawa, H., and Kano, S., 1984, Characteristics of the overland flood flows and the  
sedimentation due to breaking of the levee in the urban area: *Disaster Prevention Research  
Institute Annuals at Kyoto University*, v. 27, p. 497–511 (in Japanese with English abstract).
- Tobita, D., Kashiwaya, K., Kakinuma, T., and Takeda, A., 2015, study on sedimentation on flood  
plain during levee breach: *Japan Society of Civil Engineers Journal, Ser. B1 (Hydraulic  
Engineering)*, v. 71, p. 1291–1296 (in Japanese with English abstract).
- Toonen, W.H.J., Asselen, S.V., Stouthamer, E., and Smith, N.D., 2016, Depositional development of  
the Muskeg Lake crevasse splay in the Cumberland Marshes (Canada): *Earth Surface  
Processes and Landforms*, v. 41, p. 117–129, doi:10.1002/esp.3791.

- Wessel, P., Luis, J.F., Uieda, L., Scharroo, R., Wobbe, F., Smith, W.H.F., Tian, D., 2019, The Generic Mapping Tools version 6. *Geochemistry, Geophysics, Geosystems*, v. 20, p. 5556–5564, doi: 10.1029/2019gc008515.
- Widera, M., Chomiak, L., and Wachocki, R., 2023, Distinct types of crevasse splays formed in the area of Middle Miocene mires, central Poland: Insights from geological mapping and facies analysis: *Sedimentary Geology*, v. 443, no. 106300, doi:10.1016/j.sedgeo.2022.106300.
- Wright, L.D., 1973, sediment transport and deposition at river mouths: A synthesis: *Geological Society of America, Bulletin*, v. 88, p. 857–868, doi:10.1130/0016-7606(1977)88<857:STADAR>2.0.CO;2.
- Yamada, M., Naruse, H., Kuroda, Y., Kato, T., Matsuda, Y., Shinozaki, T., and Tokiwa, T., 2023, Features of crevasse splay deposits and sedimentary processes associated with levee breaching due to the October 2019 flood of the Chikuma River, Central Japan: *Natural Hazards*, doi: 10.1007/s11069-023-06122-7.
- Yamasaka, M., and Kubota, M., 2002, Flood flow at the steep gradient river and the deposition of sediments following it: *Advances in River Engineering*, v. 8, p. 225–230 (in Japanese with English abstract).
- Yu, M., Wei, H., Liang, Y., and Zhao, Y., 2013, Investigation of non-cohesive levee breach by overtopping flow: *Journal of Hydrodynamics*, v. 25, p. 572–579, doi:10.1016/S1001-6058(11)60398-4.

Yuill, B.T., Khadka, A.K., Pereira, J., Allison, M.A., and Meselhe, E.A., 2016, Morphodynamics of the erosional phase of crevasse-splay evolution and implications for river sediment diversion function: *Geomorphology*, v. 259, p. 12–29, doi:10.1016/j.geomorph.2016.02.005.

### THE CAPTIONS OF FIGURES AND TABLES

Fig. 1.— Drone image showing the breached levee, crevasse channel, and crevasse-splay deposit associated with the October 2019 flooding of the Chikuma River in Nagano Prefecture, central Japan (provided by the Geospatial Information Authority of Japan). The house with black roof in the bottom left corner of the image is approximately 6–7 m high.

Fig. 2.— Experimental facilities. The grid interval of the floodplain is 10 cm (Runs 1–3) and 5 cm (Runs 4–6).

Fig. 3.— The experimental procedures of three breach patterns A–C. The acrylic board controlled the water level in the flume at the downstream edge.

Fig. 4.— Experimental deposits in Runs 1–6.

Fig. 5.— The formation process of the crevasse-splay deposits with the shift in the crevasse channel direction in Run 4. **A)** 20 s after the flow overflowing started. **B)** 5 s, **C)** 30 s, and **D)** 120 s after the levee breach.

Fig. 6.— Variation in flow velocity in the crevasse channel in Runs 4 and 6.

Fig. 7.— Orthophotos of experimental deposits and digital elevation model of the crevasse-splay

deposit measured by image analysis in **A)** Run 2, **B)** Run 3, and **C)** Run 5.

Fig. 8.— Experimental deposit in Run 4. **A)** Orthophoto. **B)** Digital elevation model of the crevasse-splay deposit measured by image analysis. **C)** Volume per unit area (5 cm grid) measured by sampling. The variation along the transect is shown in Fig. 10. **D)** Ratio of green sand in the total.

Fig. 9.— Experimental deposit in Run 6. **A)** Orthophoto. **B)** Digital elevation model of the crevasse-splay deposit measured by image analysis. **C)** Volume per unit area (5 cm grid) measured by sampling. The variation along the transect is shown in Fig. 10. **D)** Ratio of green sand in the total.

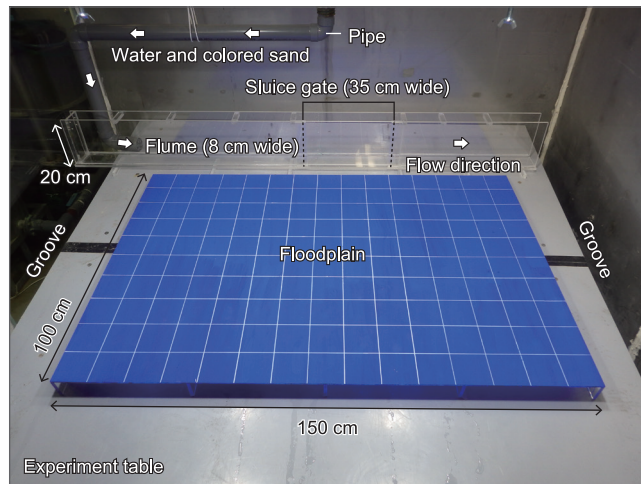
Fig. 10.— Volume per unit area variation along the transects parallel (P–P') and perpendicular (T–T') to the main channel in Runs 4 and 6.

Table 1.— *Experiment conditions. Breaching patterns A–C are explained in the main text and Fig.*

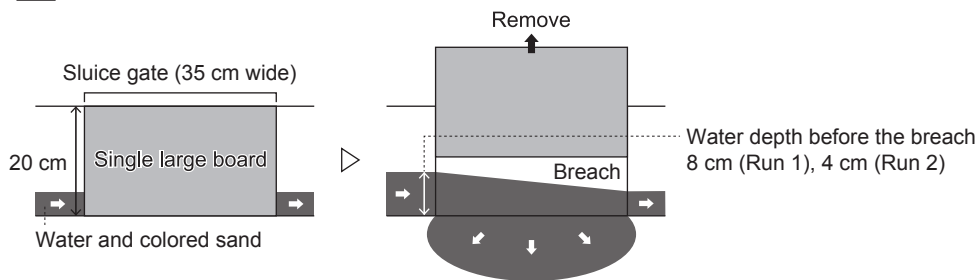
3. *Times indicate the elapsed time after the experiment started.*

Table 2.— *Comparison of hydraulic conditions in the experiments and in the actual river (Chikuma River); grain size of fine sediment in the Chikuma River is not given here because the fine-grained material in the Chikuma River exhibited a broad grain size distribution and flocculation may have occurred.*

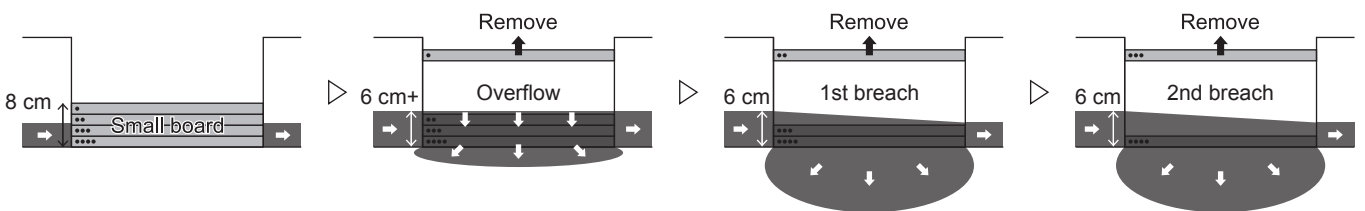




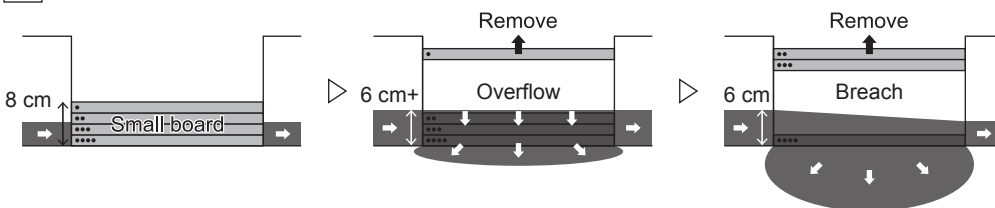
**A Pattern A (Runs 1–2: instantaneous breaching)**

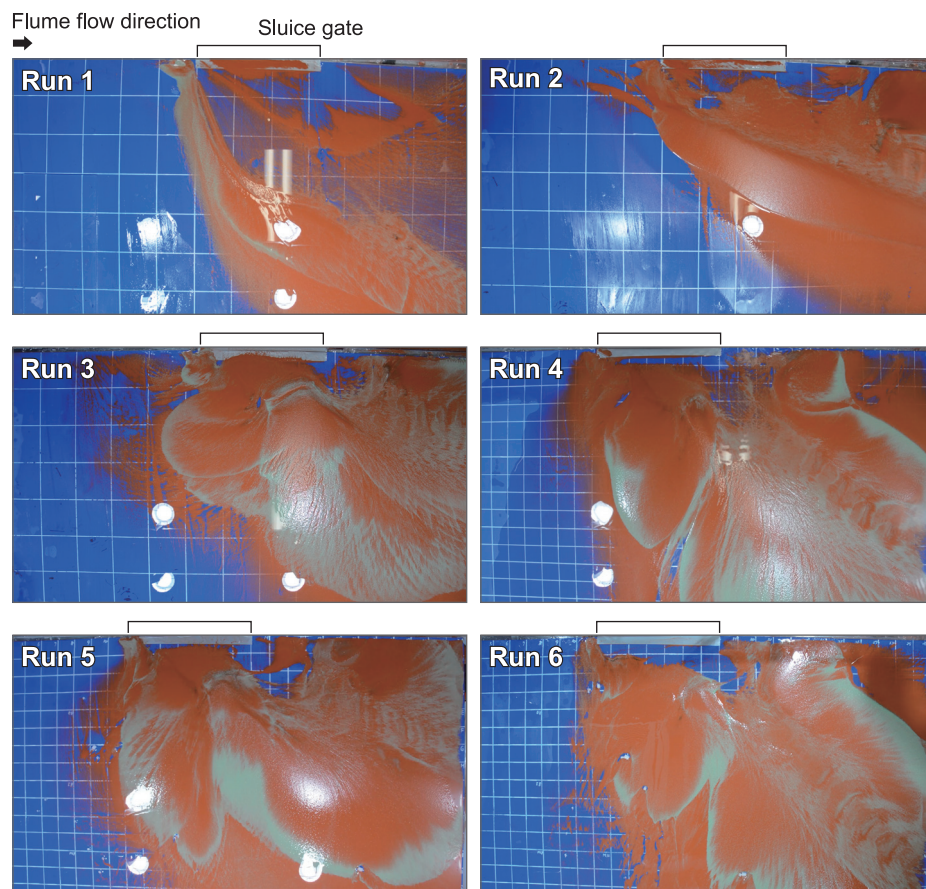


**B Pattern B (Run 3: gradual breaching)**

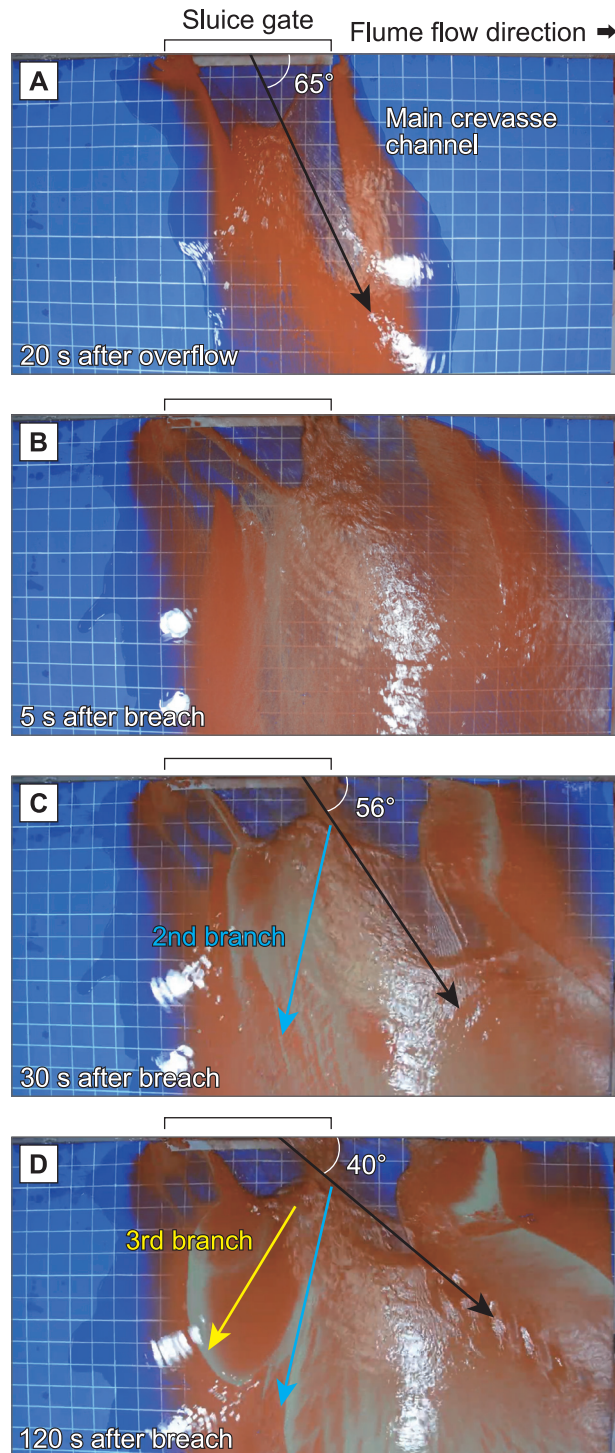


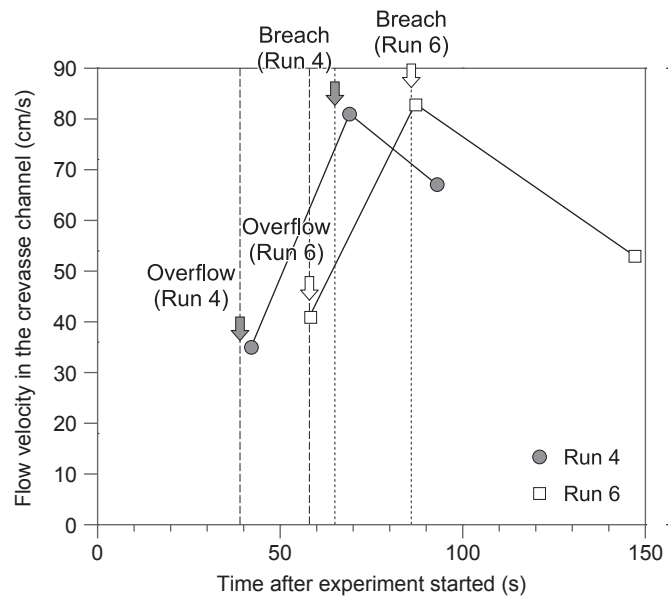
**C Pattern C (Runs 4–6: overflow to breach)**

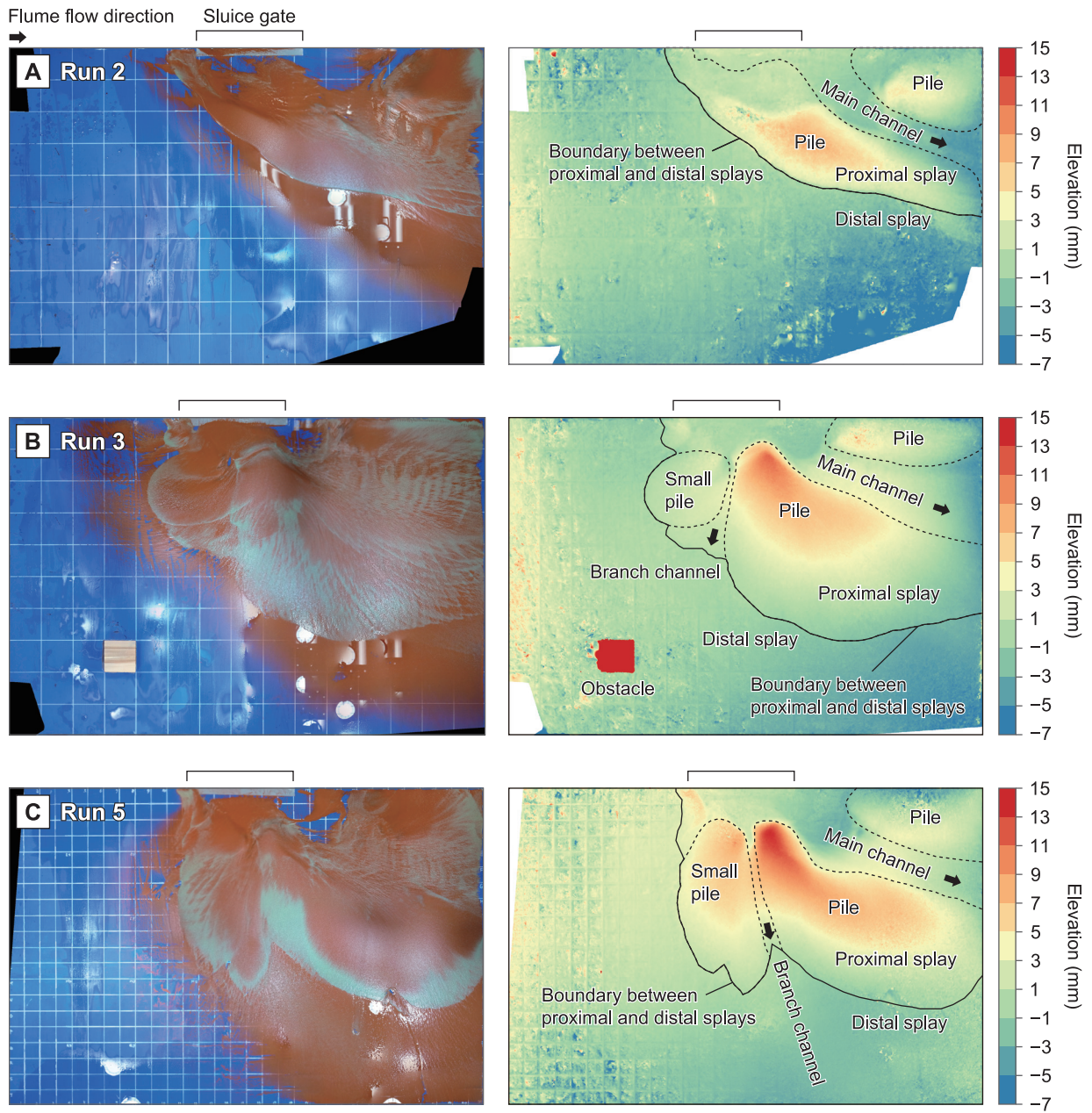


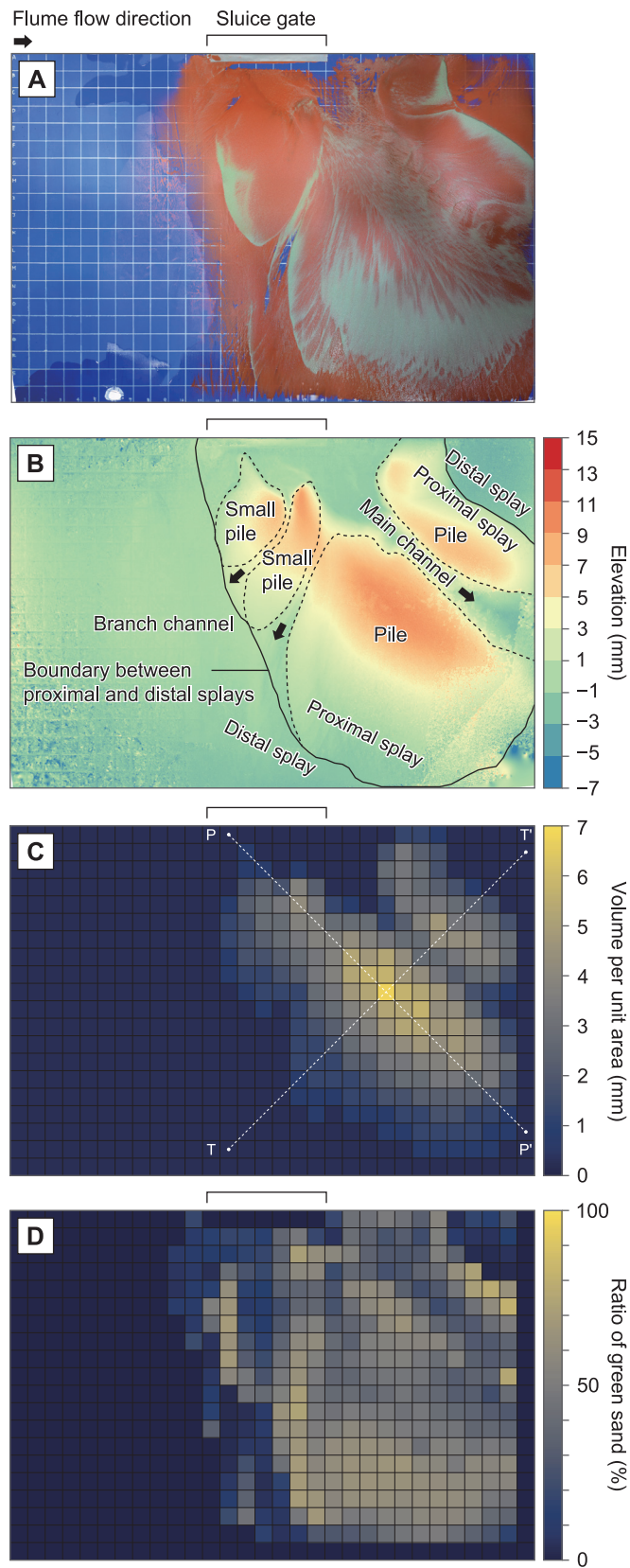




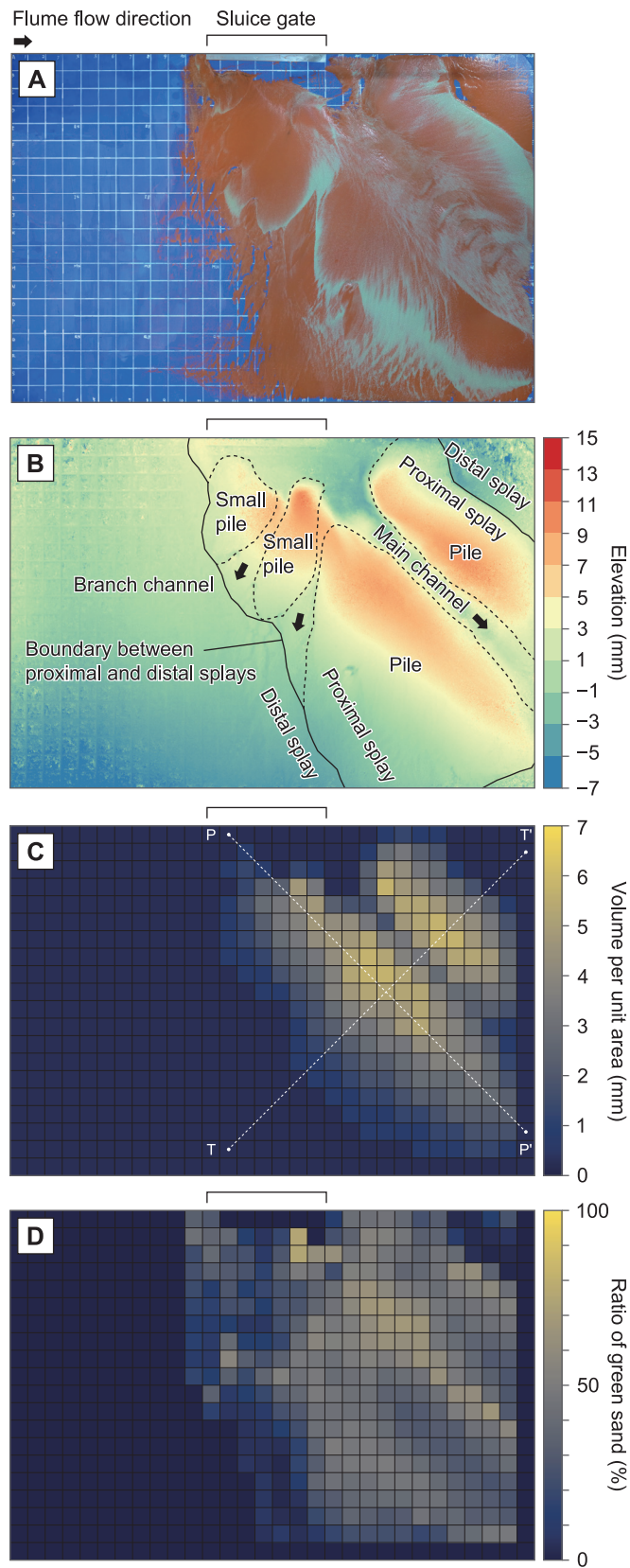












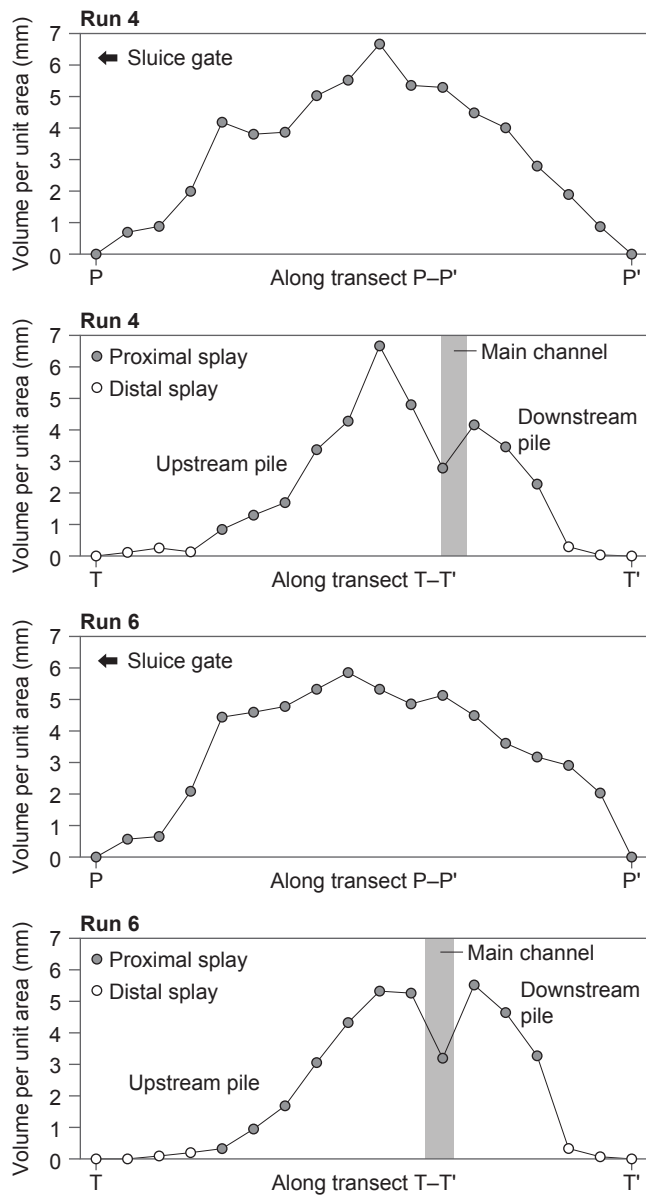


Table 1

Experiment name	Water temperature [°C]	Breach pattern	Floodplain tilt [%]	Water depth at overflow [cm]	Water depth just before breach [cm]	
Run 1	21.5	A	A	Flat	–	8
Run 2	20.2	A	A	Flat	–	4
Run 3	21.3	B	B	Flat	6+	6 (1st), 6 (2nd)
Run 4	22.4	C	–1.4 to –1.0	Flat	6+	6
Run 5	23.0	C	C	Flat	6+	6
Run 6	22.0	C	C	Flat	6+	6

Start of overflow [s]	Start of levee breach [s]	Stop of water flow [s]	Concentration in tank [%]	Concentration in downstream edge [%]	Grid interval [cm]
–	–	52	126	2.21	–
–	–	52	220	1.90	–
105	116 (1st), 124 (2nd)	–	223	2.33	–
39	–	66	226	1.20	–
33	–	62	174	2.28	0.47
58	–	86	228	1.33	1.33